Renewable Energy 78 (2015) 132–140

Contents lists available at ScienceDirect

Renewable Energy

journal homepage: www.elsevier.com/locate/renene

Three-float broad-band resonant line absorber with surge for wave energy conversion

P. Stansby [a, *], E. Carpintero Moreno [a], T. Stallard [a], A. Maggi [b]

[a] School of Mechanical, Aerospace and Civil Engineering, University of Manchester, Manchester M13 9PL, UK
[b] Cammell Laird, Birkenhead CH41 9BP, UK

ARTICLE INFO

Article history:
Received 12 March 2014
Accepted 24 December 2014
Available online 20 January 2015

Keywords:
Wave energy
Line absorber
Resonance
Heave
Surge
Pitch

ABSTRACT

A line absorber consisting of three cylindrical floats is shown to have high crest capture widths for wave energy conversion across a broad band of frequencies. The bow, mid and stern floats are small, medium and large respectively; the floats are spaced about half a wavelength apart so that forces and motion of adjacent floats are substantially in anti-phase. The bow and mid float are rigidly connected by a beam and a beam from the stern float is connected to a hinge above the mid float for power take off. The draft of the stern float enables heave resonance at a prominent wave frequency and the smaller draft of the mid float provides resonance at a somewhat lower frequency. Experimental results at about 1:8 scale show capture widths greater than 25% of a wavelength in regular waves and greater than 20% of a wavelength in irregular waves across a broad range of wave periods. A time-stepping model for regular waves with coefficients from linear diffraction theory showed similar power prediction with a generic drag coefficient of 1.8. The model shows the importance of surge forcing and heave resonance. The model also shows that reducing drag coefficient will increase capture width.

1. Introduction

Many devices have been developed for wave energy extraction and principles are well described in Ref. [4] and more recently in Ref. [2]. Here we give a brief review to provide some context for this study. Point absorbers are single devices moving in heave, pitch or surge or some combination. Resonance amplifies power generation such that the theoretical maxima in terms of capture width (of a wave crest) are $1/2\pi$, $1/\pi$ and $1/\pi$ wavelengths respectively. Examples of heaving point absorbers are Wavebob [23], WaveStar [24], Archimedes Wave Swing [15], CETO [17], Buldra [22], Manchester Bobber [10]; examples of surging and pitching devices are PS Frog [6], Oyster [14] and Langlee [19]. Response to resonance is generally narrow band although this may be broadened through latching control, e.g. Ref. [1]. To be effective most devices are designed for deployment within arrays, either separately tethered to the bed or from a fixed platform. In another form of point absorption wave motion is transmitted to an air column, driving oscillatory air motion through a turbine, usually a Wells turbine rotating in one direction, e.g. Mighty Whale [16], Ocean Energy [20].

Another concept is based on line absorption with Pelamis [21] the most notable example. The device consists of a number of longitudinal cylindrical segments, aligned with the wave direction, connected by hinges at which power is taken off. A segment is typically half a wavelength long so the pitching motion is maximised. The device is floating with a mooring and is usually about two wavelengths long. This has the potential to exceed the capture widths of single point absorber. A different form of line absorber known as Anaconda [18] has the form of a flexible submerged tube designed so that a bulge of water in the tube forms due to the wave pressure and travels at the wave speed, effectively in resonance.

Some basic principles become apparent. Single devices are of limited value for large scale generation. Resonance is desirable to optimise power generation but this is a narrow band process for a single mode and geometry. In terms of engineering practicality floating moored systems are relatively easy to deploy and maintain relative to systems with fixed supporting structures. Power take off systems may take various forms with hydraulic systems quite mature, although accessibility above water level is desirable for maintenance. In this study we consider how a line absorber may accommodate various modes of motion with a range of resonance

* Corresponding author. Tel.: +44 161 306 4598.
E-mail address: p.k.stansby@manchester.ac.uk (P. Stansby).

http://dx.doi.org/10.1016/j.renene.2014.12.057

frequencies spanning predominant values of waves. To enable this three floats are used acting predominantly in anti-phase to maximise relative motion between floats and hence power output.

2. Design principles

We are here concerned with offshore wave energy conversion rather than nearshore where the resource is less; typically water depths would be at least 20 m. A moored floating system is required as fixed platforms would be prohibitively expensive in these depths. One question is: what is the greatest power which may be generated from a floating system unlimited by size or mass given that forcing frequency is determined by waves and power may only be maximised through large float mass. It is realised that power conversion is enhanced by resonance and, while this is straightforward for a single wave frequency, effective wave energy conversion requires resonance enhancement across the range of predominant wave frequencies of the chosen area, typically peak periods of 6–8 s for wind driven waves and 9–12 s for swell waves. Different modes of motion may be excited; here we are concerned with heave, pitch and surge and these may have different resonant frequencies for each float and the excitation of different modes may be superimposed further enhancing power generation. It is recognised that surge will not resonate without hydrodynamic stiffness (due to hydrostatic pressure restoring force) but forcing could enhance power output. The converter should be effective in irregular (random), directional seas and this is consistent with the requirement of resonant response with different modes over a range of regular wave frequencies, at least on the basis of linear superposition.

In order for a large floating mass to generate power it must be connected to another float or to the sea bed with power resulting from the relative motion. Here we are concerned with a floating, moored system for ease of deployment so the motion must be relative to another float and this is maximised if the motions are in anti-phase. The spacing between two floats should thus be about half the predominant wavelength. It will be shown that pitch excitation on a single float is small relative to heave and surge. In order to optimise geometry for power two floats moving only in heave in anti-phase were initially considered. Subsequently a system comprising three floats excited in heave, pitch and surge was analysed. A linear analysis with diffraction coefficients from WAMIT [13] is described in the Appendix, giving an analytical solution for power and response for two floats in heave.

For floats to be moving in anti-phase forcing is likely to be effective over a length of up to $L/4$ where L is wavelength. As the maximum diameter will have maximum mass and hence generate maximum force and power the diameter of the stern float was chosen to be approximately $L/4$; the force will be effectively inertial and determined by the wave phase. This simple criterion is not refined further in the present study. Experiments will be described which have been undertaken in a large basin (35 m long $\times$ 15.5 m wide and 2.9 m deep) with wave periods varying around 2.4 s, from 2 s to 3.2 s. We thus use these conditions to describe the dimensions of the geometric configurations. The large stern float is given a diameter of 2 m and a draft of 0.95 m giving a heave resonance period of 2.4 s in isolation (using added mass from diffraction theory). We want the floating system to head naturally (passively) into the wave direction and it is desirable for the stern float to be bigger than the bow float hence giving a larger wave drag. At this stage we refer to the bow float as float 2 and the stern as float 3 because a float further upwave, which will be float 1, is introduced later. To cover a range of wave periods we set a target resonance period for the bow float of 2 s which requires a draft of 0.6 m for a range of diameters. With a centre-to-centre spacing of 4 m maximum power is obtained with bow float diameter $D_2 = 1.5$ m approximately for 1 m $< D <$ 2 m. In undertaking these heave optimisations mechanical damping was varied to give maximum power; this occurred when close to the radiation damping of the large float. Both resonant periods are only slightly affected by the proximity of the other float. For $T = 2.4$ s the maximum power was only slightly dependent on draft in the range 0.5 m–0.75 m. A diameter of 1.5 m and draft of 0.6 m were thus chosen. An example of the dependence of peak power on wave period and mechanical damping is shown in Fig. A1 with drag coefficient $C_D = 1.8$ which will be seen later to give good agreement with experiment for the final three body configuration. This configuration was tested at smaller lab scale (1/5 of scale described above) with two horizontal beams with hinges at each end on central vertical columns fixed on each float, the columns and beams effectively forming a parallelogram. The system responded in heave at resonance but off resonance heave motion was replaced by a coupled pitch motion with much reduced relative motion and hence power and the alignment of the two bodies could veer away from the wave direction. This option is clearly not of much practical value. However further advantage may be taken of anti-phase motion by rigidly connecting a further float 1 upwave of float 2 at a spacing also of about half a wavelength; this now becomes the bow float. This float may be relatively small so as not to diffract wave motion from the downwave floats and thus reduce their relative motion. The configuration is shown in Fig. 1. There is a single hinge above the mid float for power take off. In this configuration it is apparent that relative pitch between the two rigidly connected floats 1 and 2 and the stern float 3 will provide rotation in addition to the relative heave motion between the two upwave floats 1 and 2 (bow and mid) and the downwave float 3 (stern). It is further apparent that surge forcing on the mid float 2 and stern float 3 will be in anti-phase further potentially increasing rotation about the hinge (due to their moment about the hinge) although there is no hydrodynamic stiffness in surge to enable resonance.

The three-float system is quite complex. The heave optimisation for the two larger bodies is intended as a useful starting point. The small bow float 1 has a diameter of half the large float 3, of 1 m, and a draft of 0.35 m. This gives a resonant heave period of 1.6 s but this is of little significance. A range of float spacing and diameter was tested at lab scale (1:40) and it was found that reducing spacing of floats 1 and 2 reduced power slightly. Having a slightly smaller bow float diameter of 0.4 D_3 had little effect. A hinge point of 0.95 m above mean water level was near optimum based on laboratory scale tests. These effects were for both regular and irregular waves. It has to be remembered that results are also dependent on mass distribution and the nature of the power take off. At full scale the mass distribution will be determined by naval architecture design methods for floating offshore structures. The power take off here is idealised as a linear damper and this would be optimised hydraulically at full scale, possibly using a form of latching and accumulators for storage. Furthermore the base of the bodies considered here is essentially flat with rounded corners to reduce drag. This is for simplicity of construction and would be practical for deployment. However if drag has a significant effect on power the radius of curvature of the corners could be increased with a hemisphere as the limiting shape.

The intention here is to establish the potential for enhanced power output with forcing due to heave, pitch and surge and heave and pitch resonance. Experiments have been undertaken with the geometric configuration described above. A linear mathematical model has also been developed for regular waves to assess the relative importance of heave, pitch and surge, and also the effect of viscous drag. Comparison with experiment will assess the value of a model with hydrodynamic coefficients from linear diffraction

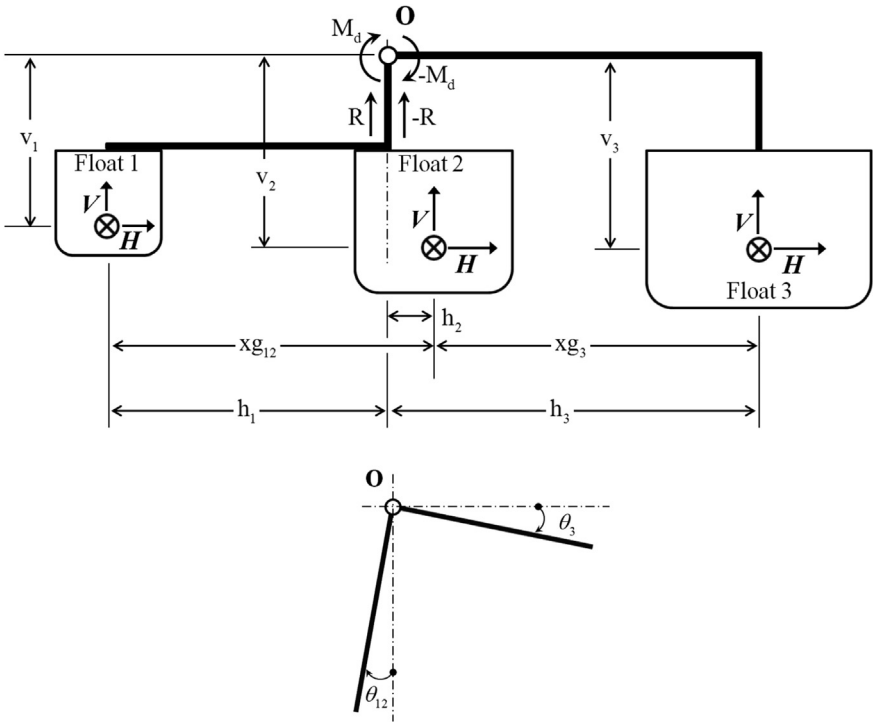

Fig. 1. Definition sketch for mathematical model.

theory. More refined optimisation would benefit from a more complete nonlinear model.

3. Linear mathematical model

The model is derived from first principles and general theoretical background is given in Ref. [7]. The damping moment M_d about O is defined by the relative angle $\theta_r = \theta_{12} - \theta_3$

$$M_d = -B_d\dot{\theta}_r \tag{1}$$

H, V and M are the horizontal and vertical forces and moment on bodies 1, 2, 3. H, V, M contain all hydrodynamic forces including radiation damping, added mass and restoring forces and drag forces. Bodies rotate about O and O is moving.

Taking moments about O:

For rigid body 12 (1 and 2 combined)

$$m_1\ddot{z}_1h_1 - m_1\ddot{x}_1v_1 - m_2\ddot{z}_2h_2 - m_2\ddot{x}_2v_2 + \sum m_i\ddot{z}_ih_i + \sum m_i\ddot{x}_iv_i - I_{12}\ddot{\theta}_{12} = M_1 + M_2 + M_d + V_1h_1 - V_2h_2 - H_1v_1 - H_2v_2 \tag{2}$$

where m and I are mass and inertia of each float and m_i, x_i, z_i correspond to additional masses above the floats, e.g. beams.

For body 3

$$-m_3\ddot{x}_3v_3 - m_3\ddot{z}_3h_3 + \sum m_i\ddot{z}_ih_i + \sum m_i\ddot{x}_iv_i + I_3\ddot{\theta}_3 = M_3 - M_d - V_3h_3 - H_3V_3 \tag{3}$$

For the whole system in the z direction with no net force (vertical and horizontal) or moment at the hinge

$$m_1\ddot{z}_1 + m_2\ddot{z}_2 + m_3\ddot{z}_3 + \sum m_i\ddot{z}_i = V_1 + V_2 + V_3 \tag{4}$$

And for the whole system in x direction with no net force or moment at the hinge

$$m_1\ddot{x}_1 + m_2\ddot{x}_2 + m_3\ddot{x}_3 + \sum m_i\ddot{x}_i = H_1 + H_2 + H_3 \tag{5}$$

In relation to O position x_O, z_O we have

$$\left.\begin{aligned} x_1 &= x_O - v_1\theta_{12} \\ z_1 &= z_O + h_1\theta_{12} \\ x_2 &= x_O - v_2\theta_{12} \\ z_2 &= z_O - h_2\theta_{12} \\ x_3 &= x_O - v_3\theta_3 \\ z_3 &= z_O - h_3\theta_3 \end{aligned}\right\} \tag{6}$$

The restoring have force and pitch moment for a single float are given by: $V_{rest} = -\rho g\pi r^2 z$ and $M_{rest} = -\rho g\pi\frac{r^4}{4}\theta$ where r is float radius.

The equations are solved with second-order time-stepping. First we solve for θ_{12}, θ_3 by substituting equation (6) above in the moment equations (2) and (3) and using estimates for $\ddot{x_O}$, $\ddot{z_O}$. Then we substitute θ_{12}, θ_3 into equations (4) and (5) and solve for x_O, z_O using estimates for θ_{12}, θ_3. This is iterated to convergence in a time step. Simple updating enabled convergence with the mechanical damping required to simulate the experimental tests but not with very low damping which was not investigated further.

Hence we obtain θ_{12} and θ_3 and x_O, z_O and power $= M_d\dot{\theta}_r$.

Table 1

	WAMIT notation		
Body	1	2	3
Surge	1	7	13
Heave	3	9	15
Pitch	5	11	17

Hydrodynamic moments and forces are defined using WAMIT notation as Table 1.

Pitch moments are given by:

For body 12 $\theta_{12} = \theta_1 = \theta_2$

$$M_1 + M_2 = M_{D5} + M_{D11} - \begin{bmatrix} A_{5,5} & A_{5,11} & A_{5,17} \\ A_{11,5} & A_{11,11} & A_{11,17} \end{bmatrix} \begin{bmatrix} \ddot{\theta}_1 \\ \ddot{\theta}_2 \\ \ddot{\theta}_3 \end{bmatrix} - \begin{bmatrix} B_{5,5} & B_{5,11} & B_{5,17} \\ B_{11,5} & B_{11,11} & B_{11,17} \end{bmatrix} \begin{bmatrix} \dot{\theta}_1 \\ \dot{\theta}_2 \\ \dot{\theta}_3 \end{bmatrix} - \begin{bmatrix} A_{5,1} & A_{5,7} & A_{5,13} \\ A_{11,1} & A_{11,7} & A_{11,13} \end{bmatrix} \begin{bmatrix} \ddot{x}_1 \\ \ddot{x}_2 \\ \ddot{x}_3 \end{bmatrix} - \begin{bmatrix} B_{5,1} & B_{5,7} & B_{5,13} \\ B_{11,1} & B_{11,7} & B_{11,13} \end{bmatrix} \begin{bmatrix} \dot{x}_1 \\ \dot{x}_2 \\ \dot{x}_3 \end{bmatrix} - \begin{bmatrix} A_{5,3} & A_{5,9} & A_{5,15} \\ A_{11,3} & A_{11,9} & A_{11,15} \end{bmatrix} \begin{bmatrix} \ddot{z}_1 \\ \ddot{z}_2 \\ \ddot{z}_3 \end{bmatrix} - \begin{bmatrix} B_{5,3} & B_{5,9} & B_{5,15} \\ B_{11,3} & B_{11,9} & B_{11,15} \end{bmatrix} \begin{bmatrix} \dot{z}_1 \\ \dot{z}_2 \\ \dot{z}_3 \end{bmatrix} - M_{drag12} + M_{rest1} + M_{rest2}$$

where $M_{drag12} = V_{drag1}h_1 - V_{drag2}\,h_2 - H_{drag1}v_1 - H_{drag2}\,v_2$, M_D is diffraction moment, A is added mass coefficient, B is radiation damping coefficient and vertical and horizontal drag forces V_{drag} and H_{drag} are defined below.

For body 3

$$M_3 = M_{D17} - \begin{bmatrix} A_{17,5} & A_{17,11} & A_{17,17} \end{bmatrix} \begin{bmatrix} \ddot{\theta}_1 \\ \ddot{\theta}_2 \\ \ddot{\theta}_3 \end{bmatrix} - \begin{bmatrix} B_{17,5} & B_{17,11} & B_{17,17} \end{bmatrix} \begin{bmatrix} \dot{\theta}_1 \\ \dot{\theta}_2 \\ \dot{\theta}_3 \end{bmatrix} - \begin{bmatrix} A_{17,1} & A_{17,7} & A_{17,13} \end{bmatrix} \begin{bmatrix} \ddot{x}_1 \\ \ddot{x}_2 \\ \ddot{x}_3 \end{bmatrix} - \begin{bmatrix} B_{17,1} & B_{17,7} & B_{17,13} \end{bmatrix} \begin{bmatrix} \dot{x}_1 \\ \dot{x}_2 \\ \dot{x}_3 \end{bmatrix} - \begin{bmatrix} A_{17,3} & A_{17,9} & A_{17,15} \end{bmatrix} \begin{bmatrix} \ddot{z}_1 \\ \ddot{z}_2 \\ \ddot{z}_3 \end{bmatrix} - \begin{bmatrix} B_{17,3} & B_{17,9} & B_{17,15} \end{bmatrix} \begin{bmatrix} \dot{z}_1 \\ \dot{z}_2 \\ z_3 \end{bmatrix} - M_{drag3} + M_{rest3}$$

where $M_{drag3} = -V_{drag3}h_3 - H_{drag3}v_3$ and vertical and horizontal drag forces V_{drag3} and H_{drag3} are also defined below.

Vertical forces are defined by:

For body 12

$$V_{12} = V_1 + V_2 = V_{D3} + V_{D9} - \begin{bmatrix} A_{3,3} & A_{3,9} & A_{3,15} \\ A_{9,3} & A_{9,9} & A_{9,15} \end{bmatrix} \begin{bmatrix} \ddot{z}_1 \\ \ddot{z}_2 \\ \ddot{z}_3 \end{bmatrix} - \begin{bmatrix} B_{3,3} & B_{3,9} & B_{3,15} \\ B_{9,3} & B_{9,9} & B_{9,15} \end{bmatrix} \begin{bmatrix} \dot{z}_1 \\ \dot{z}_2 \\ \dot{z}_3 \end{bmatrix} - \begin{bmatrix} A_{3,1} & A_{3,7} & A_{3,13} \\ A_{9,1} & A_{9,7} & A_{9,13} \end{bmatrix} \begin{bmatrix} \ddot{x}_1 \\ \ddot{x}_2 \\ \ddot{x}_3 \end{bmatrix} - \begin{bmatrix} B_{3,1} & B_{3,7} & B_{3,13} \\ B_{9,1} & B_{9,7} & B_{9,13} \end{bmatrix} \begin{bmatrix} \dot{x}_1 \\ \dot{x}_2 \\ \dot{x}_3 \end{bmatrix} - \begin{bmatrix} A_{3,5} & A_{3,11} & A_{3,17} \\ A_{9,5} & A_{9,11} & A_{9,17} \end{bmatrix} \begin{bmatrix} \ddot{\theta}_1 \\ \ddot{\theta}_2 \\ \ddot{\theta}_3 \end{bmatrix} - \begin{bmatrix} B_{3,5} & B_{3,11} & B_{3,17} \\ B_{9,5} & B_{9,11} & B_{9,17} \end{bmatrix} \begin{bmatrix} \dot{\theta}_1 \\ \dot{\theta}_2 \\ \dot{\theta}_3 \end{bmatrix} - V_{drag1} - V_{drag2} + V_{rest1} + V_{rest2}$$

where $V_{drag1} = 0.5\rho\pi r_1^2 C_D \left|\dot{z}_1\right|\dot{z}_1$; $V_{drag2} = 0.5\rho\pi r_2^2 C_D \left|\dot{z}_2\right|\dot{z}_2$ and r is radius

For body 3

$$V_3 = V_{D15} - \begin{bmatrix} A_{15,3} & A_{15,9} & A_{15,15} \end{bmatrix} \begin{bmatrix} \ddot{z}_1 \\ \ddot{z}_2 \\ \ddot{z}_3 \end{bmatrix} - \begin{bmatrix} B_{15,3} & B_{15,9} & B_{15,15} \end{bmatrix} \begin{bmatrix} \dot{z}_1 \\ \dot{z}_2 \\ \dot{z}_3 \end{bmatrix} - \begin{bmatrix} A_{15,1} & A_{15,7} & A_{15,13} \end{bmatrix} \begin{bmatrix} \ddot{x}_1 \\ \ddot{x}_2 \\ \ddot{x}_3 \end{bmatrix} - \begin{bmatrix} B_{15,1} & B_{15,7} & B_{15,13} \end{bmatrix} \begin{bmatrix} \dot{x}_1 \\ \dot{x}_2 \\ \dot{x}_3 \end{bmatrix} - \begin{bmatrix} A_{15,3} & A_{15,9} & A_{15,15} \end{bmatrix} \begin{bmatrix} \ddot{z}_1 \\ \ddot{z}_2 \\ \ddot{z}_3 \end{bmatrix} - \begin{bmatrix} B_{15,3} & B_{15,9} & B_{15,15} \end{bmatrix} \begin{bmatrix} \dot{z}_1 \\ \dot{z}_2 \\ \dot{z}_3 \end{bmatrix} - V_{drag3} + V_{rest3}$$

where $V_{drag3} = 0.5\rho\pi r_3^2 C_D \left|\dot{z}_3\right|\dot{z}_3$.

Horizontal forces are defined by:

For body 12

$$H_{12} = H_1 + H_2 = H_{D1} + H_{D7} - \begin{bmatrix} A_{1,1} & A_{1,7} & A_{1,13} \\ A_{7,1} & A_{7,7} & A_{7,13} \end{bmatrix} \begin{bmatrix} \ddot{x}_1 \\ \ddot{x}_2 \\ \ddot{x}_3 \end{bmatrix} - \begin{bmatrix} B_{1,1} & B_{1,7} & B_{1,13} \\ B_{7,1} & B_{7,7} & B_{7,13} \end{bmatrix} \begin{bmatrix} \dot{x}_1 \\ \dot{x}_2 \\ \dot{x}_3 \end{bmatrix} - \begin{bmatrix} A_{1,3} & A_{1,9} & A_{1,15} \\ A_{7,3} & A_{7,9} & A_{7,15} \end{bmatrix} \begin{bmatrix} \ddot{z}_1 \\ \ddot{z}_2 \\ \ddot{z}_3 \end{bmatrix} - \begin{bmatrix} B_{1,3} & B_{1,9} & B_{1,15} \\ B_{7,3} & B_{7,9} & B_{7,15} \end{bmatrix} \begin{bmatrix} \dot{z}_1 \\ \dot{z}_2 \\ \dot{z}_3 \end{bmatrix} - \begin{bmatrix} A_{1,5} & A_{1,11} & A_{1,17} \\ A_{7,5} & A_{7,11} & A_{7,17} \end{bmatrix} \begin{bmatrix} \ddot{\theta}_1 \\ \ddot{\theta}_2 \\ \ddot{\theta}_3 \end{bmatrix} - \begin{bmatrix} B_{1,5} & B_{1,11} & B_{1,17} \\ B_{7,5} & B_{7,11} & B_{7,17} \end{bmatrix} \begin{bmatrix} \dot{\theta}_1 \\ \dot{\theta}_2 \\ \dot{\theta}_3 \end{bmatrix} - H_{drag1} - H_{drag2}$$

where $H_{drag1} = 0.5\rho d_1 D_1 C_D |\dot{x}_1|\dot{x}_1$; $H_{drag2} = 0.5\rho d_2 D_2 C_D |\dot{x}_2|\dot{x}_2$, d is draft and D is diameter

For body 3

$$H_3 = H_{D13} - \begin{bmatrix} A_{13,1} & A_{13,7} & A_{13,13} \end{bmatrix} \begin{bmatrix} \ddot{x}_1 \\ \ddot{x}_2 \\ \ddot{x}_3 \end{bmatrix} - \begin{bmatrix} B_{13,1} & B_{13,7} & B_{13,13} \end{bmatrix} \begin{bmatrix} \dot{x}_1 \\ x_2 \\ \dot{x}_3 \end{bmatrix} - \begin{bmatrix} A_{13,3} & A_{13,9} & A_{13,15} \end{bmatrix} \begin{bmatrix} \ddot{z}_1 \\ \ddot{z}_2 \\ \ddot{z}_3 \end{bmatrix} - \begin{bmatrix} B_{13,3} & B_{13,9} & B_{13,15} \end{bmatrix} \begin{bmatrix} \dot{z}_1 \\ \dot{z}_2 \\ \dot{z}_3 \end{bmatrix} - \begin{bmatrix} A_{13,5} & A_{13,11} & A_{13,17} \end{bmatrix} \begin{bmatrix} \ddot{\theta}_1 \\ \ddot{\theta}_2 \\ \ddot{\theta}_3 \end{bmatrix} - \begin{bmatrix} B_{13,5} & B_{13,11} & B_{13,17} \end{bmatrix} \begin{bmatrix} \dot{\theta}_1 \\ \dot{\theta}_2 \\ \dot{\theta}_3 \end{bmatrix} - H_{drag3}$$

where $H_{drag3} = 0.5\rho d_3 \; D_3 C_D |\dot{x}_3| \dot{x}_3$

Results comparing power with experiment are shown below.

4. Experimental results

Measurements from the basin scale experiments made at the Plymouth COAST laboratory are presented. The Ocean Wave basin is 15.5 m wide, 35 m long and a water depth of 2.9 m was used. Waves are generated by 24 hinged flap paddles. The device was fabricated in steel by Cammell Laird and the drawing with coordinate axes is shown in Fig. 2; the origins of the x and z axes are the centreline of float 1 and the base of float 3 respectively. The mass distribution is defined in Table 2 with centre of mass position denoted by x_G, z_G. The ballast comprised 25 kg bags of lead shot and their centre of mass was estimated to be 5 cm above the float base. The centres of mass of each float and beam are shown by the red circles in Fig. 2. The concentric cyan circles show the overall centre of buoyancy and the concentric red circles show the overall centre of mass. The system with a metacentric height of 0.20 m was considered sufficiently stable for the tests. Note the actuator is shown above the beam. This is merely for convenience. On a prototype this would be below the beam with a hinge attachment at deck level.

The actuator comprises a 0.4 m long hydraulic cylinder with piston (Rexroth Bosch part code CGT3MT14/50/36) driving oil around a circuit containing a valve controlling the resistive force. The required force was estimated as far as possible by scaling up from the lab scale measurements. A load cell (Force Logic Universal S-beam) at one end of the actuator shaft measures force up to a maximum of 10 kN and a displacement transducer (Penny + Giles draw wire linear sensor) measures motion; hence instantaneous power is simply obtained.

Table 2
Mass and inertia of system components.

	Mass (kg)	x_G (m)	z_G (m)
Float 1	221	0	1.037
Beam float 1 to 2	129	1.809	1.425
Float 2	633	3.933	1.052
Beam float 2 to 3	171	5.644	1.892
Float 3	1137	7.546	0.745
Actuator	25	4.560	2.150
Ballast float 2	225	4.00	0.355
Ballast float 3	1725	8.00	0.050
Combined floats 1 and 2	1223	3.05	0.954
Combined float 3	3083	7.674	0.420
Inertia about O floats 1 and 2 combined	4467 kg m^2		
Inertia about O float 3	53,005 kg m^2		

Float alignment was always close to the wave direction with a light rope attached to the bow float. Results for variation of average power P with wave height H in regular waves are shown in Fig. 3. It can be seen that power is closely proportional to H^2 for all periods, T. It is apparent that maximum average power occurs at $T = 2.5$–2.6 s rather than 2.40 s as expected with a heave added mass coefficient of 0.52 from WAMIT for float 3. Further tests undertaken with an isolated float freely responding in heave in still water gave a measured period of oscillation of 2.50 s which implies an added mass coefficient of 0.63. Since the effect of adjacent floats is very small, about 3%, the difference must be due to viscous effects increasing added mass but this does not completely explain the experimental value slightly greater than 2.5 s. It should be noted that the WAMIT results had converged with up to 1710 panels used. Fig. 4 shows the time variation of surface elevation η without the device in position, relative angle θ_r, moment M_d or couple at the

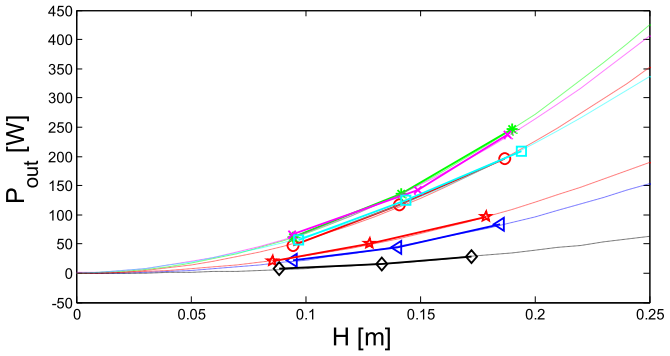

Fig. 3. Variation of average power out for T = 2.2 (◁), 2.4 (○), 2.5 (*), 2.6 (×), 2.8 (□), 3.0 (☆) and 3.2 s (◊). The solid lines show experimental results and dashed lines quadratic fits through origin.

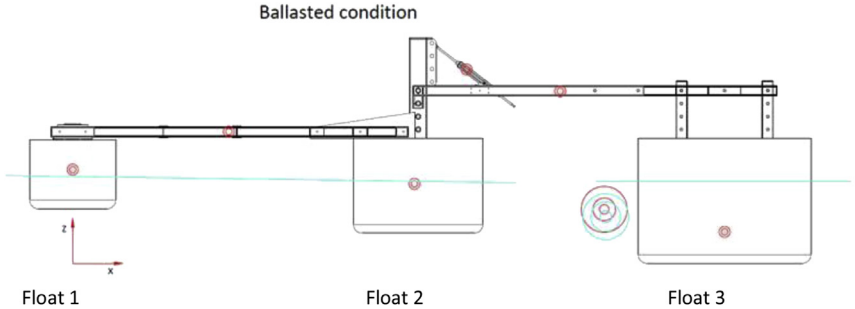

Fig. 2. Engineering diagram of system showing centres of mass of floats and beams and overall centre of mass (centre concentric red circles) and buoyancy (centre concentric cyan circles). The horizontal cyan line is the water level. (For interpretation of the references to colour in this figure legend, the reader is referred to the web version of this article.)

hinge obtained from the force, power P and $B_d = M_d/\dot{\theta}_r$. B_d values are not shown for values of $\left|\dot{\theta}_r\right|$ less than 10% of maximum value to avoid dividing by small values. For a perfect linear damper B_d would be constant and this is far from the case with a mean value of approximately 2553 Nms in this case, determined from $\int M_d dt / \int \dot{\theta} dt$. The second half of each test was analysed to give power values. The peak values of B_d are increasing, possibly due to oil heating, but this has negligible influence on regularity of response. Amplitude modulation is evident in all plots. Small irregular modulation is evident for η with $(H_{max} - H_{min})/H_{average}$ of about 7% which is indicative of small reflection, e.g. Ref. [3]. Power is proportional to H^2 giving an expected amplitude modulation of 14% while that observed is close to 20%. However the η variation is without the device in place and the device itself will cause additional reflections giving a possible explanation for the relatively large power modulation. This level of wave reflection is difficult to avoid.

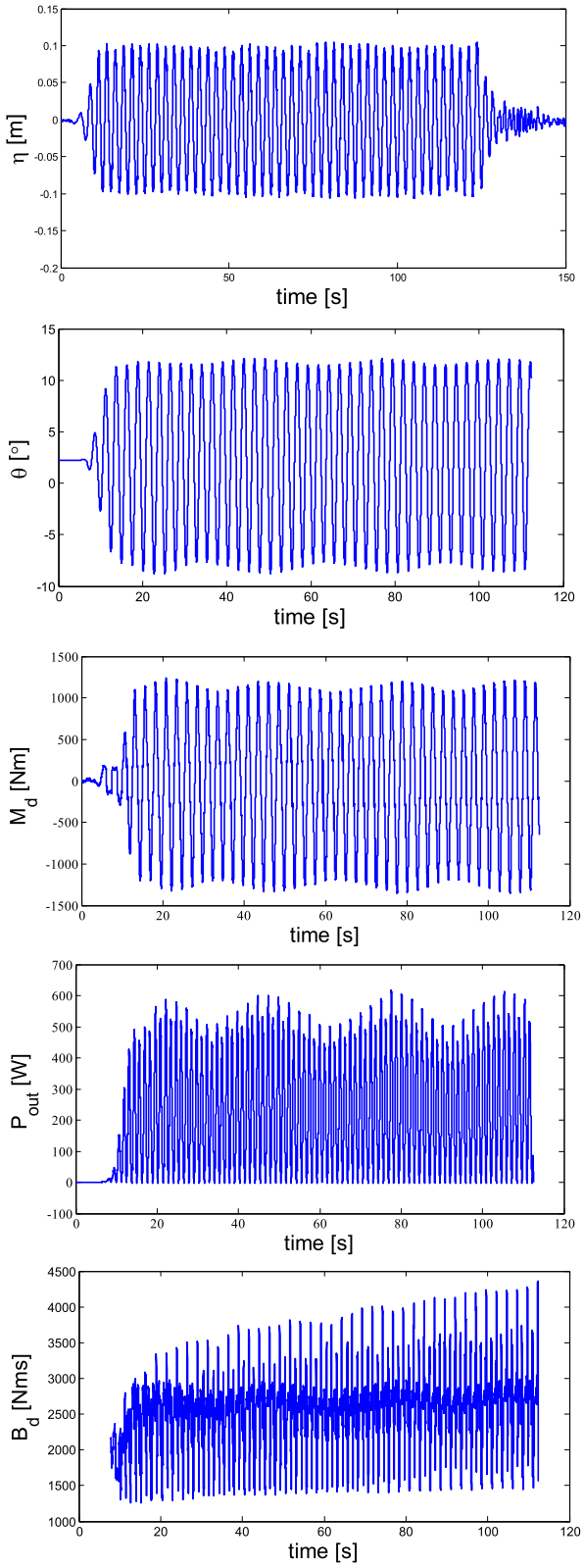

Fig. 4. Variations of surface elevation η without device in place, relative angle θ_r, hinge moment M_d, power P and mechanical damping B_d with time for regular waves with $H = 0.19$ m and $T = 2.5$ s.

The same exercise was undertaken for irregular waves. The JONSWAP spectrum was used with a spectral peakedness factor $\gamma = 3.3$. Runs of 3 min duration were used and some runs of 10 min duration were also undertaken showing negligible change in average power. The variations of average power with significant wave height H_s are shown in Fig. 5. Again it can be seen from quadratic fits that power is closely proportional to H_s^2.

Fig. 6 shows the time variation of relative angle θ_r, moment M_d or couple at the hinge obtained from the measured force, power P and $B_d = M_d/\dot{\theta}_r$. B_d has an average value of 2256 Nms in this case.

It is informative to show power in terms of crest capture width in terms of wavelength to compare with idealised values for single bodies. The formula for wave power per metre for regular waves based on linear theory is given by $P = 1/8\rho g H^2 c_g$ with group celerity $c_g = \frac{c}{2}\left(1 + \frac{2kh}{\sinh(2kh)}\right)$ where c is wave celerity, h is depth and k is wave number and for irregular waves is given to a close approximation by $P = \frac{1}{2}\left(\frac{1}{8}\rho g H_s^2 c_g\right)$ where k and c are based on the energy period T_e (=$0.78T_p$ for $\gamma = 1$ and $0.84T_p$ for $\gamma = 3.3$ where γ is the spectral peakedness factor in the JONSWAP spectrum). The formula is exact for deep water and is within 12% for the wave conditions investigated here.

The resulting capture widths are shown in Fig. 7 as a proportion of wavelength. Note the wave height values stated in the caption vary slightly with period as values resulting from a given target were slightly period dependent.

It can be seen that the curves collapse for both regular and random waves. Broad band response is apparent in both cases and the particularly broad band response in irregular waves is desirable with a maximum close to 25% of a wavelength only slightly below that for regular waves. For a single point absorber in heave the

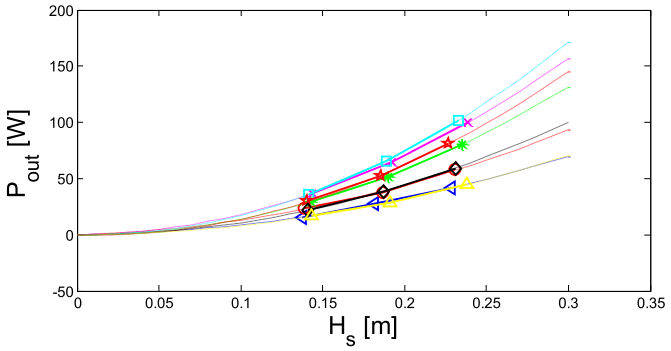

Fig. 5. Variation of average power out for $T_p = 2.2$ (◁), 2.4 (○), 2.5 (*), 2.6 (×), 2.8 (□), 3.0 (☆), 3.2 (◇) and 3.4 s (△). The solid lines show experimental results and dashed lines quadratic fits.

theoretical maximum capture width at resonance is 16% and for pitch and surge is 32%. The capture width is about 14% of the width of the tank.

Finally the effect of spectral peakedness factor $\gamma = 1$ is considered, giving the Pierson-Moskowitz spectrum which is a special case of the JONSWAP spectrum. Also real seas are rarely unidirectional and spectra with directional spreading are considered with spreading factors $s = 5$ (large spread) and 30 (small spread); s $= \infty$ corresponds to unidirectional waves. The directional spreading parameter s defines a spreading function of cosine shape, $\cos^s(\theta)$, the standard in OCEAN software [8].

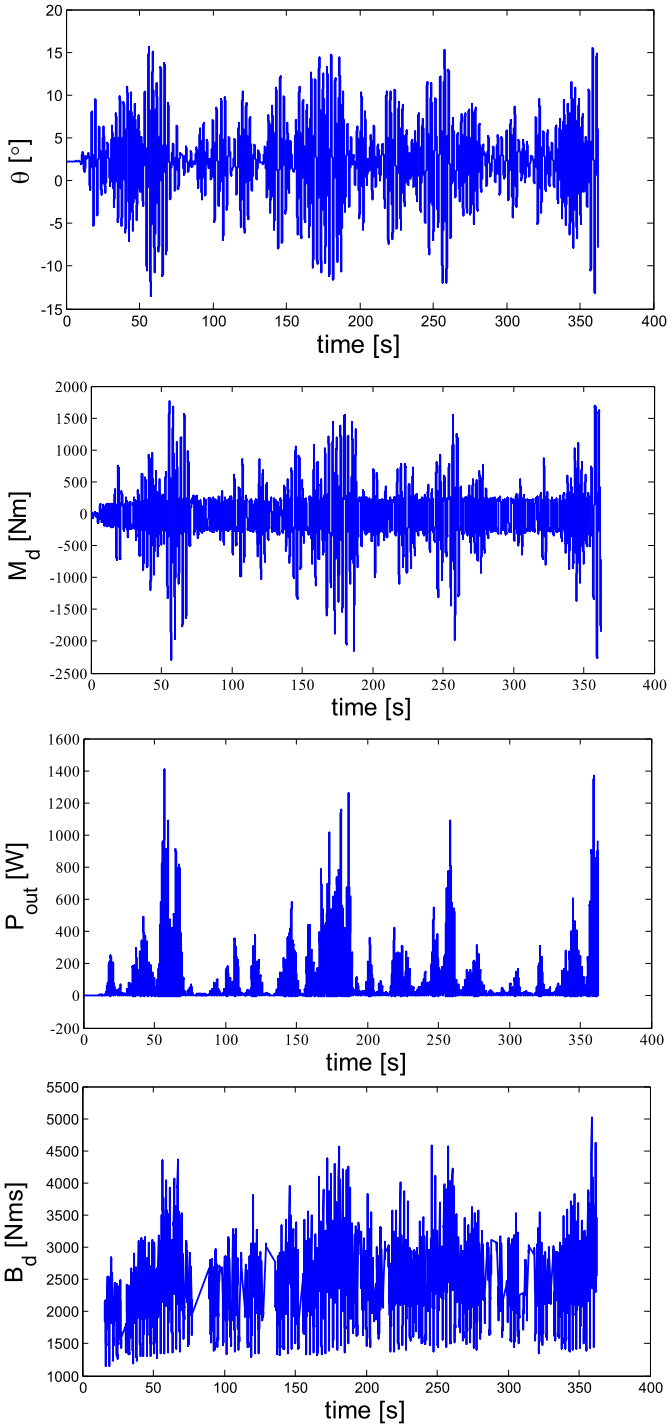

Fig. 6. Variations of relative angle θ_r, hinge moment M, power P and mechanical damping B_d with time for random waves with $H_s = 0.23$ m and $T_p = 2.8$ s.

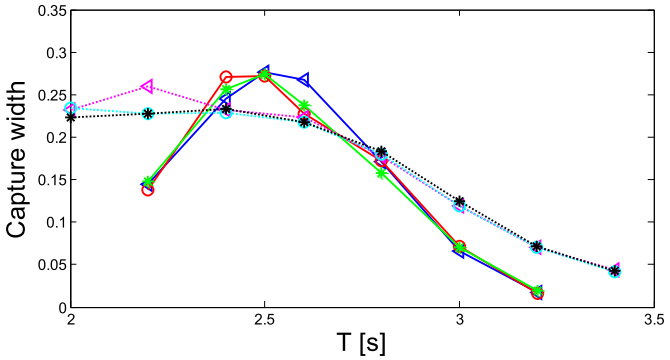

Fig. 7. Variation of capture width as proportion of wavelength (based on energy period in irregular waves) with period for regular waves (full lines) with $H \approx 0.095$ (◁), 0.14 (○), 0.19 m (*) and with peak period in irregular waves (dashed lines) for $H_s \approx 0.14$ (◁), 0.19 (○), 0.23 m (*).

Results are shown in Fig. 8 for $H_s \approx 0.19$ m. It can be seen that spread seas slightly increase power output. Reducing the spectral peakedness factor from 3.3 to 1 reduces maximum power by about 25% although this is less away from the maximum.

5. Discussion

The aim of this development is to show how different modes of forcing and variable heave resonance may combine to magnify power output from a line absorber and provide the broad band response required to capture energy from the wave climate of an offshore site. This is achieved here with three cylindrical floats of different diameter and draft with spacing of about half a wavelength. The stern float is as large as possible, while capturing the wave phase, with mass and hence draft selected to resonate in heave at a prominent wave period. This diameter has been specified as about a quarter of a typical wavelength giving inertial forcing and it is expected that this could be optimised further. The bow and mid floats are rigidly connected with a hinge above the mid float connecting a beam to the stern float. Power take off or damping in these experiments is from the oscillatory rotation of this beam about the supporting column on the mid float. Although the system is complex hydrodynamically it is quite simple mechanically. Wave drag, particularly from the large stern float, is intended to cause the floats to be in line with the wave direction. The bow float is relatively small but provides a lever arm generating a moment at the

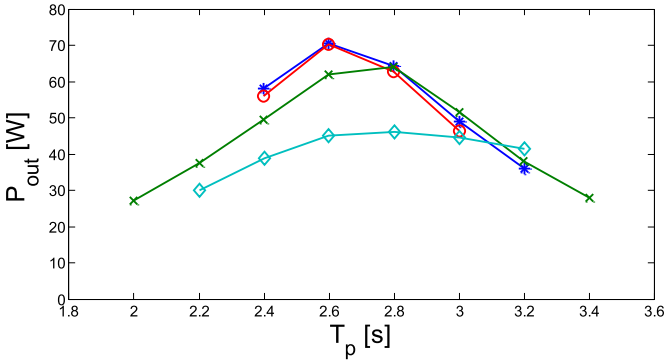

Fig. 8. Variation of power with peak period T_p for random waves with $H_s \approx 0.19$ m with different spread parameter s and spectral peakedness factor γ in JONSWAP spectrum: $\gamma = 3.3$: $s = 30$(*); $s = 5$(○); $s = \infty$(x); $\gamma = 1$: $s = \infty$(◇).

hinge. The mid float draft gives a lower resonant period than the stern float capturing energy from lower periods within the wave climate and the diameter is specified to optimise energy capture for two floats in heave. Experiments show that this alignment heads closely into the wave direction and there is the intended broad band performance in regular and random waves. The capture width in irregular waves is 20–25% of the wavelength for the energy period over a peak period range of ±20% from a mid value, e.g. about 6–8 s at full scale.

A linear mathematical model for regular waves provides some insight into how hydrodynamic forcing causes energy capture. The model with WAMIT coefficients for added mass, radiation damping and excitation forces gives average power similar to experiment using a drag coefficient C_D of 1.8 which is consistent with bodies in oscillatory flow, e.g. Ref. [5]. However in the present study C_D is treated as a tuning parameter with the same value for heave and surge motion although there would certainly be physical differences for these modes. Also drag coefficient will depend on the magnitude of motion and we have chosen a small wave height case for comparison to be consistent with linear assumptions. A constant linear damping parameter B_d has been assumed while experiments show significant variation. The maximum powers are at a slightly lower period than in the experiments, around 2.4 s rather than 2.5–2.6 s, shown in Fig. 9. To assess the influence of viscosity on heave added mass and hence natural period some tests were undertaken with the large float in isolation freely oscillating in still water. This indicated an added mass about 17% greater than prediction from linear diffraction analysis explaining that the difference from the period at maximum power is partially attributed to viscous effects. Another example of viscous effects causing an increase in added mass is the circular cylinder in low amplitude oscillatory flow, e.g. Ref. [9], although viscous effects generally cause a reduction for large amplitudes. The additional difference of about 0.05 s remains unexplained but of course three body motion is more complex with pitch as well as heave and nonlinear effects could also be significant with amplitudes of motion about 20% of draft or diameter even for the small wave height case considered.

The relatively simple model captures important aspects of the physics. It shows that the average power with $C_D = 1$ is about 60% higher than with $C_D = 1.8$ around resonance, shown in Fig. 9, suggesting that reduction in drag will certainly be beneficial. This would require a more rounded base which might not be as convenient for construction and deployment but that would need to be investigated. The hypothetical maximum theoretical power capture with $C_D = 0$ gives a capture width of 75% of the wavelength or three times that obtained in the experiments reported. The theoretical maximum for a single device is approximately 32% in surge or pitch and 16% in heave. The absolute maximum for three floats acting individually would thus be 96%, requiring resonance in all three floats which would be difficult to achieve. Here the situation is more complex with heave generating pitch on two floats, heave resonance on a third, prominent surge forcing and pitch on individual floats. The theoretical maximum capture width of 75% wavelength may be considered a high value.

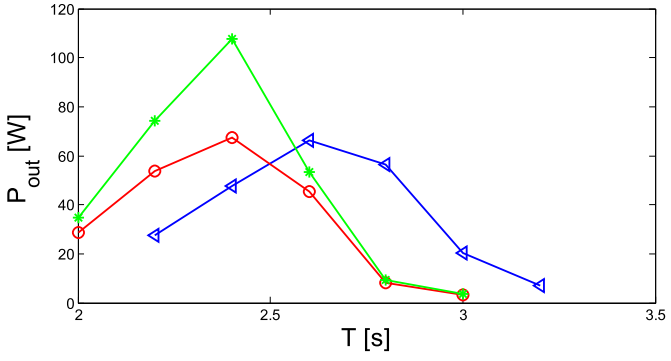

Fig. 9. Power from experiments with $H \approx 0.095$ m (◁) compared with the linear model with $C_D = 1.8$ (○), $C_D = 1$ (*).

The influence of mechanical damping coefficient B_d may also be investigated with the model. At resonance ($T = 2.4$ s) with $B_d = 2553$ Nms the average power of 67 W is increased to close to 90 W with B_d in the range 4000–8000 Nms, more than 30% increase. This increase will probably also occur with irregular waves while a control system would further improve power output.

The model enables assessment of the contribution of forcing in specific modes to the overall power output; this is of course impossible experimentally but simple in a model. Removing heave excitation reduced average power by about 46% close to resonance, removing surge excitation reduced power by about 57% while removing pitch reduced power by only 12%. However pitch excitation is here defined as due to the moment about individual floats while the two rigidly connected floats will also appear to pitch as a result of heave forces on each acting approximately in anti-phase.

Survivability in extreme waves remains to be investigated. However some tests were undertaken in the Plymouth Ocean basin with the largest waves available, approximately 0.7 m in height. The damper was disconnected and the system showed good sea keeping with the head seas under investigation. The upper float surfaces became periodically submerged causing splashing and damping, as investigated for a single float in Ref. [12]. With the PTO disconnected the forces on the beam between the bigger floats will be small and the stresses on the beam connecting the smaller floats could be the most critical.

The capture width variation with period provides an ideal method for determining energy yield from a scatter diagram. This is clearly site dependent and is not undertaken here but a typical full scale estimate of power generation is of interest. Typical average H_s and T_e for the south west of England are 2 m and 5.5 s respectively. This gives a scale of 1:8 approximately in relation to present tests. With a capture width of 20% of a wavelength for the energy period, increased by a factor of 1.3 with optimised mechanical damping, the average power generation would be about 140 kW. On the other hand some parts of the world have predominant swell waves which are quite regular. With a wave height of 1 m and period of 10 s an appropriately scaled system would yield average power of 520 kW (based on 25% wavelength capture width for regular waves). Since device size is proportional to wavelength, hence square of period, this device would need to be 3.3 times larger than the device considered above which has dimensions suitable for wind waves with $T_e = 5.5$ s.

It is clear that the performance may be optimised further, by increasing damping, controlling the power take off, reducing drag and also further optimising the float configuration and geometry. The three float linear model includes many interactions but omits nonlinear hydrostatic effects, some viscous effects and 2nd order effects. The latter are known to be significant for wave trapping between offshore columns and will be the subject for future analysis. Full scale viscous effects are most difficult to model as high Reynolds number turbulent boundary layers with separation would need to be resolved. However linear diffraction analysis for regular waves is valuable and may be extended to irregular waves through impulse response functions.

In terms of practical application, energy yield needs to be optimised for a given location, survivability in extreme waves needs to be demonstrated and the full scale system needs to be costed to assess commercial viability. The present work has shown that the power potential for a line absorber in real seas may be greater than

previously understood. While the hydrodynamics are complex the present analysis provides a basis for optimisation.

6. Conclusions

A line absorber with three cylindrical floats has been proposed with the bow and mid float rigidly connected by a beam and a hinge for power take off above the mid float connects a beam to the stern float. The floats increase in draft and diameter from bow to stern and the system heads naturally into waves. The spacing between adjacent floats is about half a wavelength so the forcing and motion are in anti-phase. Experiments and mathematical modelling indicate how heave resonance of stern and mid floats and surge forcing combine to give high capture widths in regular and irregular waves across a broad frequency range typical of an offshore site. The system may be optimised further by using more streamlined floats reducing drag, by optimising the mechanical damping and control of power take off, and possibly by further optimising dimensions. The intention is to produce a system generating electricity from large-scale deployment at a cost competitive with offshore and possibly onshore wind.

Acknowledgements

We acknowledge generous support from Cammell Laird on fabrication and naval architecture analysis through D. Williams and from Rexroth Bosch for provision of the hydraulic actuator through L. Verdegen, from CONAYCT for the scholarship for the second author and EPSRC for the Supergen Marine Challenge 2 grant StepWEC (EP/K012487/1). The Plymouth COAST laboratory provided a high quality facility and technical service. The patent application has been made by P.Stansby of M4 WavePower Ltd [11]. The reviewers made some helpful comments.

Appendix. Analytical two-body heave analysis

For two bodies oscillating in heave only, denoted by mode 3 on body 1 and mode 9 on body 2

$$(\boldsymbol{M}+\boldsymbol{A})\ddot{\boldsymbol{z}} = -(\boldsymbol{B}+\boldsymbol{B_d})\dot{\boldsymbol{z}} - \frac{1}{2}\rho A C_D \dot{\boldsymbol{z}}|\dot{\boldsymbol{z}}| - \rho g A \boldsymbol{z} + \boldsymbol{F}$$

where mass $\mathbf{M} = \begin{bmatrix} M_1 & 0 \\ 0 & M_2 \end{bmatrix}$, added mass $\mathbf{A} = \begin{bmatrix} A_{33} & A_{39} \\ A_{93} & A_{99} \end{bmatrix}$, radiation damping $\mathbf{B} = \begin{bmatrix} B_{33} & B_{39} \\ B_{93} & B_{99} \end{bmatrix}$, vertical force $\mathbf{F} = \begin{bmatrix} F_3 \\ F_9 \end{bmatrix}$, and F_3 accounts for effect of body 2 on body 1 and F_9 accounts for effect of body 1 on body 2. ρgA is sometimes known as hydrodynamic stiffness S where A is cross-sectional area normal to oscillation. The coefficients and forces are obtained from WAMIT. The mechanical damping with coefficient B_d is due to relative velocity and adding the effect of linearised drag gives $\mathbf{B_{dd}} = \begin{bmatrix} -B_d - A_1 k|\dot{z}_1| & B_d \\ B_d & -B_d - A_2 k|\dot{z}_2| \end{bmatrix}$ where $k = \frac{1}{2}\rho C_D \pi/4$. The complex velocity amplitude $\dot{\boldsymbol{z}}_0 = \frac{\mathbf{F_0}}{\left[\mathbf{B}+\mathbf{B_{dd}}+\omega\left(\mathbf{M}+\mathbf{A}-\frac{\mathbf{S}}{\omega^2}\right)\boldsymbol{i}\right]}$ where $\mathbf{F_0}$ is the complex force amplitude and ω is the angular wave frequency. Finally the power out $P_{out} = B_d(\dot{z}_2 - \dot{z}_1)^2$. This equation set was solved iteratively using Matlab. For the case with diameters of 1.5 m and 2 m, a spacing of 4 m and drafts of 0.6 m and 0.95 m respectively the contour map for peak power as a function of frequency and mechanical damping is shown in Fig. A1 for a wave height of 0.1 m and $C_D = 1.8$ to correspond with the value found to give good agreement with three-body tank tests. The maximum average power of 21 W occurs with B_d close to the radiation damping value on the large float (857 Ns/m). Note B_d here is different from that for rotational motion about the hinge for the three-body case.

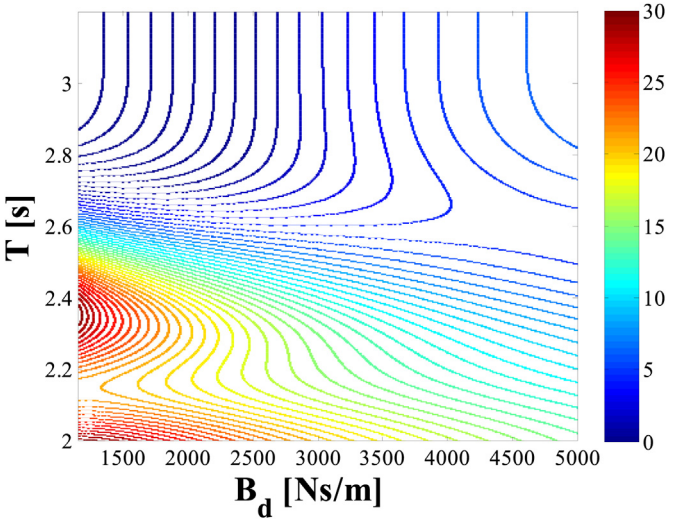

Fig. A1. Peak power contours as function of mechanical damping coefficient B_d and wave period T for two bodies in heave.

References

[1] Babarit A, Clément AH. Optimal latching control for a wave energy device in regular and irregular waves. Appl Ocean Res 2006;28:77–91.
[2] Cruz J. Ocean wave energy. New York: Springer; 2008.
[3] Dean RG, Dalrymple RA. Water wave mechanics for engineers and scientists. Singapore: World Scientific Press; 1991.
[4] Falnes J. Ocean waves and oscillating systems. Cambridge: Cambridge University Press; 2002.
[5] Faltinsen OM. Sea loads on ships and offshore structures. Cambridge: Cambridge University Press; 1993.
[6] McCabe AP, Bradshaw A, Meadowcroft JAC, Aggidis G. Developments in the design of the PS Frog Mk 5 wave energy converter. Renew Energy 2006;31(2):141–51.
[7] Mei CC. The applied dynamics of ocean surface waves. Singapore: World Scientific Publishing; 1989.
[8] Rogers D, Bolton King G. Wave generation using ocean and wave. 1997. version 3.62.
[9] Sarpkaya T. Force on a circular cylinder in viscous oscillatory flow at low Keulegan-Carpenter numbers. J Fluid Mech 1986;165:61–71.
[10] Stansby P. Robust wave energy device evaluation and design. Carbon Trust Report 2004-10-1867-7. 2004.
[11] Stansby P. Surge based wave energy converter PCT/GB2013/050787. 2013.
[12] Stallard TJ, Weller SD, Stansby PK. Limiting heave response of a wave energy device by draft adjustment with upper surface (special issue) Appl Ocean Res 2009;31(4):282–9.
[13] WAMIT. WAMIT user manual versions 6.2, 6.2PC, 6.2S. 6.2SPC. WAMIT Inc; 2004. www.wamit.com.
[14] www.aquamarine.com.
[15] www.awsocean.com.
[16] www.caddet-re.org.
[17] www.carnegiewave.com.
[18] www.energy.soton.ac.uk/anaconda-wave-energy-converter-concept.
[19] www.langleewavepower.com.
[20] www.oceanenergy.ie.
[21] www.pelamiswave.com.
[22] www.seewec.org.
[23] www.wavebob.com.
[24] www.WaveStarEnergy.com.